

INITIAL TEST BED FOR VERY HIGH EFFICIENCY SOLAR CELLS

Allen Barnett¹, Xiaoting Wang¹, Nick Waite¹, Paola Murcia¹, Christiana Honsberg¹, Doug Kirkpatrick², Dan Laubacher³, Fouad Kiamilev¹, Keith Goossen¹, Mark Wanlass⁴, Myles Steiner⁴, Richard Schwartz⁵, Jeff Gray⁵, Allen Gray⁶, Paul Sharps⁶, Keith Emery⁴, Larry Kazmerski⁴

¹University of Delaware, Newark, DE, United States; ²Defense Advanced Research Projects Agency (DARPA), Arlington, VA; ³E. I. du Pont de Nemours and Company, Wilmington, DE; ⁴National Renewable Energy Laboratory (NREL), Golden, CO; ⁵Purdue University, West Lafayette, IN; ⁶Emcore, Albuquerque, NM.

ABSTRACT

Very High Efficiency Solar Cell (VHESC) program is developing integrated optical system–photovoltaic modules for portable applications that operate at greater than 50 percent efficiency. We are integrating the optical design with the solar cell design, and we have entered previously unoccupied design space [1]. A test bed for rapid development and verification of performance of subsystems is also being developed. The results and analysis of the first complete integrated optics and solar cells on this test bed are reported. The demonstration has achieved efficiency greater than 36%. Analysis shows a direct path to efficiencies greater than 40%. These initial results have not been verified by NREL or any other 3rd party. We have previously reported the sum of the solar cell efficiencies to be over 42%, and optical subsystem efficiency greater than 93% [2]. Our approach is driven by proven quantitative models for the solar cell design, the optical design and the integration of the two.

INTRODUCTION

Our group is developing high-efficiency modules based on co-design of the optics, interconnects, and solar cells. The new architecture significantly increases the design space for high-performance photovoltaic modules in terms of materials, device structures, and manufacturing technology. It affords multiple benefits, including increased theoretical efficiency, new architectures that circumvent material/cost trade-offs, improved performance from non-ideal materials, device designs that can more closely approach ideal performance limits, reduced spectral mismatch losses, and increased flexibility in material choices. An integrated optical/solar cell allows efficiency improvements while retaining low area costs and hence expands the applications for photovoltaics. The new design approach focuses first on performance, enabling the use of existing state-of-the-art photovoltaic technology to design high-performance, low-cost, multiple-junction III-Vs for the high and low energy photons while circumventing existing cost drivers through novel solar cell architectures and optical elements.

The Test Bed assembly reported in this paper is a submodule of the planned portable battery charging module. As such it provides information for the design of the final portable battery charger. The measurement

combines the solar cell efficiency with the optics (optical efficiency) to yield test bed efficiency. The highest 3rd party verified efficiency for a submodule is 27.0% [3]. The highest photovoltaic module efficiency of any type previously reported was 29.4% [4]. To date, the test bed submodules have been measured with efficiency greater than 36%, and analysis shows a direct path to efficiencies greater than 40%.

PHOTOVOLTAIC SYSTEM ARCHITECTURE

Overview

The new system architecture is based on a “parallel” or lateral optical concentrating system, which splits the incident solar spectrum into several bands and allows different optical and photovoltaic elements in each band. The optics and the cells are co-designed to achieve the maximum conversion efficiency of the module. An example of the photovoltaic system architecture is shown in Figure 1. The new architecture integrates optical and solar cell design, allowing a much broader choice of materials and circumventing many existing cost drivers. This architecture enables the inclusion of multiple other innovations and leads to higher efficiency, both at the solar cell and module levels. The optical system consists of a tiled nonimaging concentrating system, coupled with a spectral splitter that divides the solar spectrum into a given number of bands.

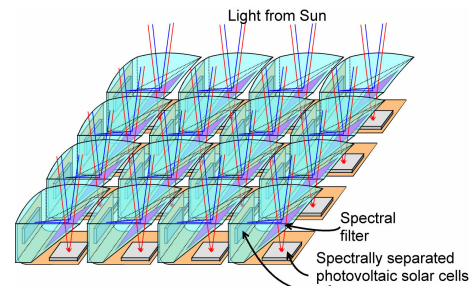


Figure 1: Schematic showing the optical elements in the lateral optics, including a static concentrator and spectral splitting [2].

The lateral solar cell architecture increases the choice of materials for multiple junction solar cells by allowing the solar cell in each spectral band to be optimized independently of the others. In this way, the lattice and current matching constraints are reduced. Further, since

the devices do not need to be series connected, spectral mismatch losses are reduced, which is important for tandems in terrestrial environments. Finally, by contacting the individual solar cells with individual voltage busses, the new architecture eliminates the need for tunnel junctions. Since each material requires unique tunnel contact metallurgy, eliminating tunnel junctions is a substantial simplification.

An additional benefit of this architecture is the opportunity to use different solar cell areas within the system, which leads to different levels of concentration of the sunlight. The concentration is defined as the aperture area that is collecting the sunlight divided by the solar cell active area.

Lateral Optical System

To achieve the benefits of the new photovoltaic system architecture, a new optical element is designed that combines a nonimaging optical concentrator (which does not require tracking and is called a *static concentrator*) with spectral splitting approaches that split the light into several spectral bands. This system is called a *parallel* or *lateral concentrator*, since solar cells are not placed vertically or optically in series. These optical elements are tiled, with the overall optical module being an affordable and manufacturable optical element that incorporates both static concentration and a dichroic element for spectral splitting.

The unique features of this optical system place an emphasis on high system optical efficiency, the use of dichroic mirrors for spectral splitting, and the design of the system to be thin enough to allow integration with other products. For example, previous approaches using static concentrators have not been practical because the optical elements are too thick for conventional modules [5,6]. Further, previous optical systems, particularly spectral splitters, have suffered from reduced optical efficiencies. The use of an integrated system and small area dichroic mirrors allows both the efficiency and cost issues to be overcome. The optical system does not require tracking and has no moving parts.

The critical metric for the module development is module efficiency. This which consists of two factors: (1) optical efficiency, which is the amount of sunlight that is directed to the solar cells, weighted by the energy in each band of sunlight; and (2) the sum of the power from each solar cell.

Optics Design

The most advanced optical design is based on non-symmetric, nonimaging optics, tiled into an array. The central issues in the optical system are the optical efficiency and the amount of time over which the sunlight remains focused on the solar cells (tracking time). Since

the module is designed for portable battery charging applications, the time in which the module is stationary is relatively short. The tracking time or the field of view is limited by the size of the photovoltaic cells and “beam walk,” or the tendency of the spot of energy on the detector to move as the angle of the sun changes. Overall, the concentrators are designed to accept light for several hours, rather than over the course of an entire day, because the modules are designed for portable electronics.

The transmission efficiency of the optical system under weighted average AM1.5G spectrum is designed to be greater than 90%.

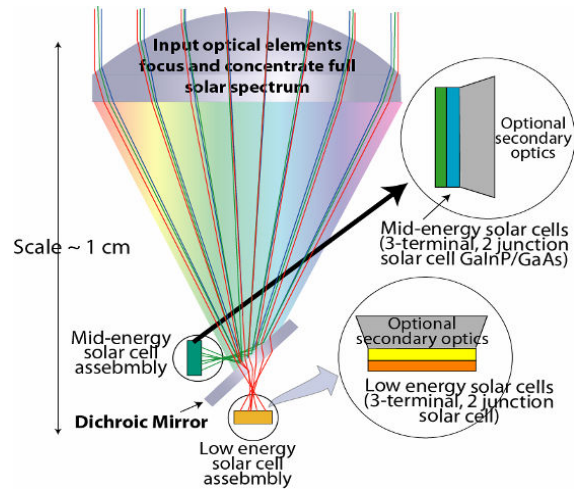


Figure 2: Schematic of the assembled submodule.

FLEXIBLE TEST BED FOR EFFICIENCY MEASUREMENT

Overview

The Flexible Test Bed is an integrated optical/solar cell system that allows testing in sunlight of (1) the individual solar cells, (2) the solar cells in combination with individual optical components, and (3) the full module. Optical components and solar cells can be readily interchanged.

In addition to providing a platform for testing the submodule and its components in sunlight, the data leads to rapid submodule performance improvements based on identification of losses, leading to “loss minimization”. This is based on the counting of the available photons and the resultant current for each energy gap. These photons can then be integrated with the measured external quantum efficiency and compared to the measured current.

A basic proof of concept (POC) design was developed and tested, which consists of four

components, as shown in Figure 2. These are (1) a front lens (2) a dichroic mirror that reflects the light above 1.43 eV and passes light below this energy (3) a 3-terminal Mid-Energy (M-E) solar cell which converts sunlight to electricity with energies above 1.43 eV and (4) a 3-terminal Low-Energy (L-E) solar cell which converts sunlight to electricity at energies above 0.72 eV. Imaging optics is used for this test bed.

The optics splits the sunlight into two bins. The solar cells in each bin are in optical series and have separate electrical contacts as shown in Figure 2. This demonstrates the basic concepts of the VHESC approach. The data from the Test Bed can then be used to develop the commercial devices.

The system includes a converging lens which concentrates the direct sunlight, a dichroic mirror, which splits the whole spectrum into two sub-bands, Mid-E solar cell (solar cell with middle energy gap) and Low-E solar cell (solar cell with low energy gap), as shown in Figure 3. The test goals include efficiency test of the converging lens, dichroic mirror, solar cells, and the whole system. The efficiency test is performed outdoors.

Test System

The test system comprises four parts: solar cell carrier boards, optical assembly, electrical test instrumentation, and sun tracker.

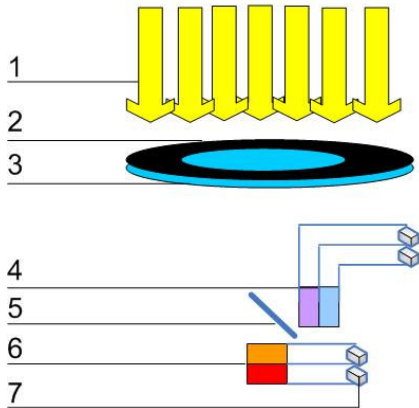


Figure 3: Flexible Test Bed integrated optical/solar system. 1. incident direct sunlight; 2. aperture; 3. converging lens; 4. Mid-E GaInP/GaAs solar cell; 5. dichroic mirror; 6,7. Low-E GaInAsP/GaInAs solar cell.

Solar Cell Carrier Board

Solar cells are mounted and wire bonded to the custom-designed solar cell carrier boards, which have a large “handle” end and a small “solar cell” end. The large end fits in the form factor of a GSM SIM card, allowing mating with off-the-shelf SIM sockets. Use of these

sockets provides screwless repeatable mechanical alignment, solderless assembly of test boards, and repeatable good electrical contact due to the “scrubbing” effect of horizontal insertion. The small end of the test board has 6 wire bond pads in a radial pattern to allow for various solar cell shapes and pad arrangements. Figure 4 shows the structure of the solar cell carrier board.

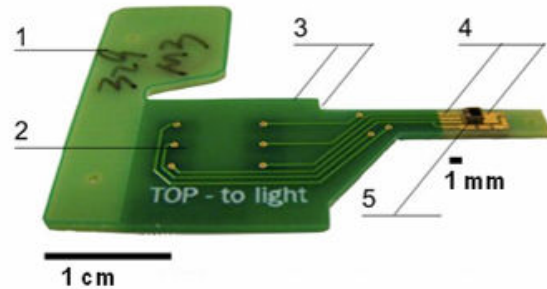


Figure 4: Flexible Test Bed solar cell carrier board. 1. handle and ID # surface; 2. SIM card contact; 3. alignment faces; 4. wire bond pad; 5. solar cell.

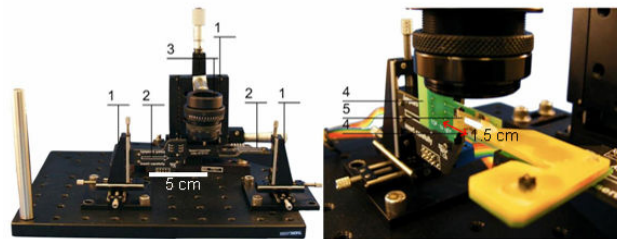


Figure 5: Flexible Test Bed optical/solar integrated system. 1. three-axis stages; 2. test board sockets; 3. lens with aperture; 4. solar cell carrier boards; 5. dichroic mirror.

Solar cell carrier boards can be inserted into the SIM sockets on the adapter boards, which are screwed into mini-sized three-axis stages as shown in figure 5.

Optical Assembly

The dichroic mirror is mounted on a similar board, which mates to the solar cell carrier board, allowing spacing to be set without the need for another three-axis stage. The converging lens is held by another three-axis stage. Figure 5 shows all the components in the optical/solar integrated system.

Sun Tracker

For the converging lens to receive sunlight and focus at the solar cells, the integrated optical/solar system should always be oriented toward the sun. The entire submodule is mounted on a camcorder tripod head

attached to an EKO robotic sun tracker. Meanwhile, a pyroheliometer is mounted on the sun tracker, which can measure the intensity of direct light. The entire setting is shown in Figure 6. As previously described, this is the imaging case.

Test Procedures and Results

The critical parameters measured include the input power from the sun, the optical efficiency, the concentration, and the power from the solar cells under 20X conditions. To achieve system efficiency, the configuration in Figure 3 is adopted. The following sections describe how each parameter is measured.

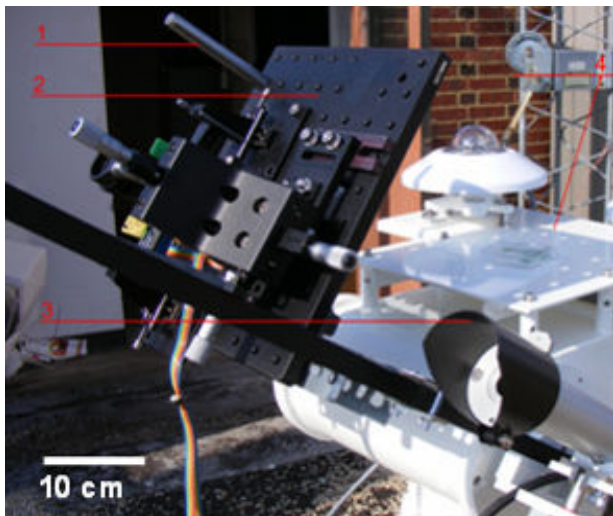


Figure 6: Flexible Test Bed entire setting. 1. The post indicates right orientation when no shadow is observed. 2. Base plate holding the entire submodule. 3. Pyroheliometer. 4. Sun tracker.

Input Radiation and Concentration Measurement

The power density of direct light can be measured from the pyroheliometer mounted on the sun tracker. The aperture on top of the converging lens used to define the light-receiving area can be measured by counting pixels in the image of aperture, as shown in Figure 7. Dimension 1 is working as a reference whose real size can be measured with electronic caliper. The area of the aperture is 21.315 mm². The incident power is the product of the aperture area and the power density measured by the pyroheliometer. The concentration is defined as the ratio of the area of light entering the lens (defined by an aperture, which is measured as shown in Figure 7 and described in the section below) and the solar cell area (1 mm²).

Output Measurement and Result Analysis

Table 1 shows the solar cell and optical efficiency results. The sub-module efficiency is the solar cell efficiency multiplied by the optical efficiency.

The optical efficiency is determined by first measuring I_{sc} (outdoors) without the lens or other optical components. This measurement is done with a collimating tube to eliminate the diffuse light. The concentration ratio is known by measuring the optical aperture and cell geometries as described above. The optical components are then inserted, and the cell I_{sc} is again measured (outdoors). Assuming that I_{sc} is linear with light intensity, the optical efficiency can be determined by the ratio of the I_{sc} measured with the lens assembly to the I_{sc} without the lens multiplied by the concentration ratio X , as shown below:

$$\eta_{optics} = \frac{I_{sc(withoutoptics)}}{I_{sc(1sun)} \cdot X} \quad (1)$$

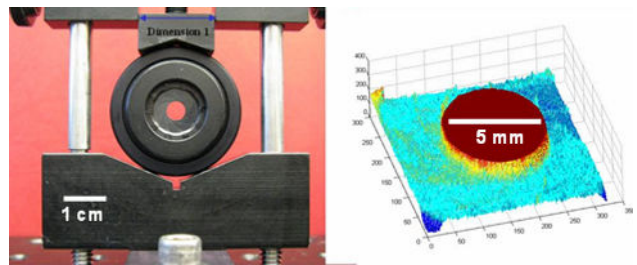


Figure 7: Image of aperture and extraction of pixel information.

The measurement with the optical components does not use a collimating tube. To verify that this does not introduce significant error, the total diffuse light was calculated assuming that the diffuse light is isotropic, using the acceptance angle of the lens, and assuming that diffuse light near the horizon can enter the solar cells. For these conditions, only 0.3% of the power incident can be attributed to diffuse light. When a collimating tube was introduced over the optics, no change in the output current of the solar cell was measured. Consequently, this part of the energy can be neglected in the first phase of efficiency measurement.

The low energy solar cells require additional considerations. First, it was found that the current from the bottom junction will increase if the top junction in the two-stack is left in an open circuit condition during that measurement. This current gain is eliminated if the top junction is held at the maximum power or short circuit. For these measurements the top junction was held at short circuit. Second, the one-sun I_{sc} measurement requires the use of a low-pass filter, since they should be illuminated only with light below 850 nm. By measuring

the I_{sc} with and without this filter, the efficiency of this filter can be determined. Measurement of the filter shows a sharp cut-off. From these measurements, the I_{sc} under one sun conditions for photons with a cut-off of 850 nm can be determined. This I_{sc} value is used in the equation above.

Table 1: Submodule Efficiency

	Solar Cell Efficiency 21.3X	Optical Efficiency	Submodule Efficiency With Optics 21.3X
Mid-E solar cell			
top	18.1	0.851	15.4
bottom	13.3	0.820	10.9
Low-E solar cell			
top	8.9	0.910	8.1
bottom	2.0	0.900	1.8
TOTAL	42.3	0.856	36.2

An optical efficiency for each junction is separately calculated and the efficiency of the overall system is separately calculated. Any sunlight that is transmitted to the Low-E solar cell and which should have been reflected to the Mid-E solar cell becomes an optical efficiency loss for the Mid-E solar cell and an optical efficiency gain for the Low-E solar cell. Accordingly the optical efficiency of the bottom junction of the Mid-E is reduced by any photons that go through to the top junction of the Low-E solar whose calculated optical efficiency is accordingly increased.

Efficiency and Power Measurements

The solar cell measurements, shown in detail in Table 2, are determined by measuring the short circuit current under outdoor one-sun conditions. The solar cells are then taken indoors. For the one-sun outdoor measurements, the light intensity from the simulator is adjusted to give the outdoor one-sun I_{sc} and the IV curve is measured. For the concentrator measurements, the light intensity is adjusted until the measured I_{sc} is the outdoor one-sun I_{sc} times the concentration ratio. The IV curve is then measured. In Table 2, a concentration ratio of 20X is used. The mounting precludes explicit cell cooling, but the IV measurements are achieved in under several seconds, and may be considered close to room temperature.

The power and efficiency measured from the solar cells in the Test Bed closely match those same measurements from the suppliers; Emcore and NREL. This leads to a good level of confidence in the accuracy of these measurements. Table 2 shows the Test Bed data (average of 4 solar cells) compared to the suppliers data (average of 5) for one sun and 20X for the Mid-E solar cells. The efficiencies are remarkably similar, with the Test Bed measuring 2.1% less than the supplier for One Sun and 3.2% less for 20 Suns (20X). Similar

detailed data was not available for the Low-E solar cell, but the efficiency measured (10.9% under a GaAs filter from the supplier) is also close to the Test Bed measurements (10.9%). The next step is calibrated measurements at the National Renewable Energy Laboratory. These measurements are not intended as calibrated measurements, but to identify the sources of error in the measurements. The close match with other measurements both indicates that the solar cells are not affected by mounting and that the solar cell measurements are not a dominant source of error.

Analysis and Path to Higher Efficiency

The major sources of measurement error are based on the measurement of the input power. The dominant sources of error are the measurement of the aperture area, the calibration of the pyroheliometer (which measures the input power), and variations in the actual sunlight when compared to the standard AM1.5D solar spectrum. The aperture measurement is the most common source of error. We estimate the possible error from this as +2%/-5% (relative). The calibration of the pyroheliometer was done by the factory and its error is estimated as +/-5% (relative). Spectral content errors were minimized by restricting the reported measurements to those conditions where the direct component of the solar radiation was greater than 900 Watts/m². There was no separate correction done for spectral changes. Other possible sources of error include the collection of diffuse light by the optical system and errors in solar cell measurement.

Analysis of Table 1 shows several paths to higher performance submodules, and even higher efficiency potential of an integrated module. Table 3 summarized the losses and ways to minimize them. The first source of the loss is the solar cells themselves. For these tests, "record" solar cells were not used. Solar cells with a nearly 1.5% absolute gain in the mid-energy range have been measured. Further, smaller improvements in the low energy solar cells, about 0.4% absolute, have been shown.

Table 1 also shows that the optical efficiencies, particularly of the top lens, is relatively low. This is no surprise, since the lens assembly has several non-optimum surfaces. An improved AR coating on both surfaces of the lens minimizes reflection losses. A conservative estimate is 0.6% absolute reduction in reflection for each surface. In addition, as with the solar cells, the test bed does not use the fully optimized dichroic mirror. An additional non-ideal source of loss is the reflection from the rear of the dichroic mirror. Together, these features allow a 1.3% absolute increase in efficiency.

The sum of these near term potential gains is 4.2% absolute, allowing a submodule efficiency of over 40%. Measurements of the several optical designs have shown 93% efficiency.

Table 2 Test Bed solar cell measurements for the Mid-E solar cells (1 mm²) compared to the supplier measurements.

	Jnct	I _{sc}	V _{oc}	FF	Jnct Eff	Tot Eff
One Sun		(μA)	(V)		(%)	(%)
Test Bed (4 cell avg)	Top	145.1	1.389	0.856	17.2	29.1
	Bot	156.1	0.938	0.811	11.9	
Emcore (5 cell avg)	Top	146.8	1.404	0.856	17.6	29.4
	Bot	140.2	0.992	0.848	11.8	
20 X	Junct	(mA)	(V)	FF	(%)	(%)
Test Bed (4 cell avg)	Top	2.90	1.475	0.848	18.1	31.5
	Bot	3.12	1.027	0.831	13.3	
Emcore (5 cell avg)	Top	2.95	1.506	0.861	19.1	32.4
	Bot	2.80	1.097	0.862	13.2	

CONCLUSIONS AND NEXT STEPS

The central approach in choosing among the expanded material design space allowed by the optical elements is first to design for performance, eliminating only those aspects fundamentally incompatible with ultimately achieving low cost, and then to design for low-cost manufacture. This strategy involves parallel approaches in the initial phases, so that success does not depend on a single approach.

The increased design space provides a path to circumventing lattice and current matching constraints imposed by monolithic, series-connected tandems. For lattice-matched (or close to lattice-matched metamorphic) tandems, only a limited number of materials are available. However, in the lateral optical approach, the materials can be chosen for their performance potential. This is particularly important for the very high energy band gaps required for the 5 and 6 junction tandems.

The results of 36.2% submodule test bed efficiency, combined with the near term path to higher submodule efficiency is a good indication of the power of the new photovoltaic architecture. The next steps are to improve the performance of the test bed and apply these concepts to a manufacturable design. The number of watt-hours delivered to the battery needs to be optimized.

Table 3: Near Term Path to Higher Submodule Efficiency

Path to Higher Test Bed Efficiency	Target Efficiency	Potential Gain (absolute)
Better solar cells		
Mid-Energy	33.0%	1.3%
Low-Energy	11.4%	0.4%
Better optics		
Higher performance lens	98.0%	1.2%
Higher efficiency dichroic mirror	93.0%	1.1%
AR coating on bottom of mirror	99.0%	0.2%
Optical Efficiency (weighted)	91.0%	
Test Bed Potential Efficiency	40.4%	4.2%

The power of the collaborative approach is demonstrated by the number and breadth of organizations that contributed to the new architectural design and implementation. The optics designs included contributions from government, universities, and industrial participants. The system reported here features two types of solar cells (4 junctions). The continued development of this co-design approach to the optics interconnects and solar cells will lead to 50% efficient modules.

ACKNOWLEDGEMENTS

This research was, in part, funded by the U.S. Government Defense Advanced Research Projects Agency under Agreement No.: HR0011-0709-0005. The views and conclusions contained in this document are those of the authors and should not be interpreted as representing the official policies, either express or implied, of the U.S. Government.

The authors thank Ramsey Hazbun from Blue Square Energy for his careful and responsive laser scribing of these new solar cell chips. The dichroic mirrors provided by Laszlo Takacs and Roger Buelow of Energy Focus.

REFERENCES

[1] Barnett, A., Honsberg, C., Kirkpatrick, D., Kurtz, S., Moore, D., Salzman, D., Schwartz, R., Gray, J., Bowden, S., Goossen, K., Haney, M., Aiken, D., Wanlass, W., Emery, K., Moriarty, T., & Kiehl, J. (2006 May). *50% Efficient Solar Cell Architectures and Designs*. Conference Record of the 2006 IEEE 4th World Photovoltaic Science and Energy Conference, Hawaii. Volume 2, 2260 -2564.

[2] Barnett, A., Kirkpatrick, D., Honsberg, C., Moore, D., Wanlass, M., Emery, K., Schwartz, R., Carlson, D., Bowden, S., Aiken, D., Gray, A., Kurtz, S., Kazmerski, L., Moriarty, T., Steiner, M., Gray, J., Davenport, T., Buelow, R., Takacs, L., Shatz, N., Bortz, J., Jani, O., Goossen, K., Kiamilev, F., Doolittle, A., Ferguson, I., Unger, B., Schmidt, G., Christensen, E. & Salzman, D. (2007, September). *Milestones toward 50% Efficient Solar Cell Modules*. Paper Presented at the 22nd European Photovoltaic Solar Energy Conference, Milan, Italy.

[3] Green, M., Emery, K., King, K.D.L., Hisikawa, Y. & Warta, W. (2006). Solar cell efficiency tables (Version 27). *Progress in Photovoltaics*, 14, 1, 45-51.

[4] Garboushian, V & Slade, A. (2007 August). *29.4% efficiency under field conditions*. Paper presented at SPIE Conference, San Diego.

[5] Winston, R., Miñano, J.C., & Benítez, P. (2005). *Nonimaging Optics*. Boston: Elsevier Academic Press.

[6] Luque, A.L. & Andreev, V.M. (2007). *Concentrator Photovoltaics*. New York: Springer.